

Clinical evaluation of ¹¹C-Met-avid pituitary lesions using a ZTE-based AC method

Gaspar Delso, Daniel Gillett, Waiel Bashari, Tomasz Matys, Iosif Mendichovszky and Mark Gurnell

Abstract— Pituitary tumours account for ~16% of central nervous system tumors and they are the second most frequently reported histology in this group. Due to their small size, pituitary surgery is challenging and precise lesion localization through imaging is therefore a critical factor for a successful outcome.

Simultaneous PET/MR is well suited for lesion identification and localization but it requires accurate attenuation correction to ensure optimal PET imaging. Atlas-based attenuation correction methods are often used for this purpose, as they overcome the difficulty of estimating bone tissue density with conventional MR sequences. However, atlas methods can only partially account for inter-patient variability.

The goal of the present study was to investigate whether direct bone measurement, by means of a zero echo time (ZTE) MR sequence, can significantly improve the accuracy of pituitary tumor imaging with PET.

Index Terms— ZTE, PET/MR, attenuation, pituitary

INTRODUCTION

The pituitary gland, or hypophysis, is an endocrine gland located at the base of the brain, suspended from the hypothalamus by a gray matter stalk. It is housed by the hypophysial fossa of the sphenoid bone, at the center of the middle cranial fossa. The pituitary gland is approximately 13 mm in diameter and 5 mm of height, weighing 500 mg. In humans, the pituitary gland consists of two main lobes, anterior and posterior, each releasing specific hormones that affect several bodily functions.

Given its key role in overall metabolic regulation, the effects of tumoral lesions in the pituitary gland can have devastating effects in both health and quality of life. Pituitary tumors include slow-growing benign pituitary adenomas, invasive pituitary adenomas -which may spread to neighboring structures- and malignant pituitary carcinomas - which may create metastases in the central nervous system or remote organs-.

According to the Central Brain Tumor Registry of the United States [1], tumors of the pituitary gland account for ~16% of central nervous system tumors (rate 3.98 per 100,000), with only a minimal fraction of these being malignant (rate 0.01 per 100,000). Tumors of the pituitary are the second most frequently reported histology (16.2%).

Treatment options for pituitary tumors include surgery, drugs and radiation therapy, with partial excision of the pituitary gland via trans-sphenoidal surgery (TSS) being the most common. The standard detection procedure is magnetic resonance imaging (MRI) of the *sella turcica* region. Recent work has shown ¹¹C-Methionine positron emission imaging (PET) to provide valuable complementary

information: E.g. to identify residual adenoma in patients with persistent acromegaly after therapy [2] or to facilitate targeted surgical therapy of corticotropin-secreting tumors in Cushing's syndrome [3], as well as radiosurgery planning and radiotherapy [4].

Hybrid Positron Emission Tomography and Magnetic Resonance Imaging (PET/MR) is an emerging modality, introduced for clinical use in 2011. There are a number of reasons suggesting that PET/MR could become the modality of choice for pituitary lesion imaging:

First, the availability of perfectly co-registered anatomical and functional data in a single examination. Given the size of the pituitary gland and its critical role in overall metabolic function, there is very little margin of error when planning partial surgical excision. Precise lesion localization and delimitation through imaging are therefore a critical success factor. Good co-registration is even more necessary when dealing with complex abnormal structures, such as the follow-up of patients not responding to surgical treatment.

Furthermore, the extremely low rate of malignancy makes this indication ideal for focused -as opposed to whole-body- imaging. Fully integrated PET and MR systems excel at this particular task, as the extended scan time required to acquire multiple complementary MR sequences can be effectively exploited by PET. The additional time can be used to either increase the quality of the acquired PET data, reduce the required radiotracer dose or perform kinetic analysis of tracer dynamics.

One of the main challenges of PET/MR imaging is attenuation correction. Quantitative PET imaging requires compensating for the signal attenuation introduced by the patient. In PET/CT scanners, this is estimated from the X-ray attenuation data provided by the computed tomography (CT) scan. In the absence of CT data, PET/MR scanners must rely on relatively complex segmentation procedures to identify different tissue classes (e.g. fat, soft tissue, lung, etc.) and assign them *a priori* attenuation coefficients [5], [6].

In the particular case of head imaging, the identification of bone tissue is a determining factor of the final PET accuracy [7]. However, MR is not an ideal modality for bone imaging: cortical bone yields signals that are weak, due to the low proton density (~20% of water), and short-lived, due to the heterogeneous structure (T2 ~ 390μs at 3T)[8]. The incorporation of anatomical atlas information into the attenuation correction process is often used to overcome this obstacle [9]-[11].

While atlas-based attenuation correction methods have been shown to result in usable PET reconstructions for routine clinical imaging [12]-[15], they are also known to conform sub-optimally to each patient's anatomical variability. Atlas methods also have a limited ability to account for off-norm anatomies, such as those caused by pathology or surgical alteration. As an alternative to the use of *a priori* anatomical models, short echo time sequences have been proposed for direct bone imaging with MR [16], [17]. In particular, 3D radial zero

G. Delso is with GE Healthcare, Waukesha, WI, USA (e-mail: gaspar.delso@ge.com).

D. Gillett and I. Mendichovszky are with the Dept of Nuclear Medicine, Addenbrooke's Hospital, Cambridge, UK.

T. Matys is with the Dept of Radiology, Cambridge University, Cambridge, UK.

W. Bashari and M. Gurnell are with the Institute of Metabolic Science, University of Cambridge & Addenbrooke's Hospital, Cambridge, UK.

echo time (ZTE) imaging has been proven to provide high-resolution isotropic images, suitable for bone segmentation [18]–[20].

The goal of the present study is to investigate whether direct bone measurement with ZTE can significantly improve the accuracy of pituitary tumor imaging in PET/MR. We hypothesize that, due to its structurally complex location, surrounded by a small bony cavity (*sella turcica*) and in close proximity to a cavity (*sphenoid sinus*), conventional atlas registration methods are not accurate enough to account for the inter-patient variability of this region.

MATERIALS AND METHODS

Data acquisition was performed at Addenbrooke's Hospital (Cambridge, UK) within the context of a sponsored study for the development of new methods for pituitary tumor diagnosis and treatment. This study was approved by the institutional review board.

A. Patients

Twenty-five subjects were recruited between June 2017 and May 2018: 10 male, 15 female; age 41 ± 14 , range 20 to 70; weight 85 ± 22 kg, range 54 to 158 kg. All subjects were adults, referred for a clinically indicated PET/CT. Exclusion criteria were the standard contraindications of MR imaging as well as claustrophobia or body habitus not compatible with the 60 cm bore of the PET/MR scanner. Of the above, 14 patients returned 28 ± 1 days later for a post-therapy session. All subjects provided signed informed consent prior to the examinations.

B. Data acquisition

All subjects were required to fast for a minimum of 4 hours prior to the injection of the radiotracer. Before the PET/CT examination, they were injected intravenously with 412 ± 39 MBq of ^{11}C -Methionine, range 301 to 442 MBq. The acquisition took place 19 ± 2 min, range 14 to 25 minutes after tracer administration

The PET/CT acquisition (Discovery 690 PET/CT, GE Healthcare) followed the site's default protocol for pituitary imaging. First, a helical CT scan was acquired: 140 kV, 220 mAs, matrix size 512×512 , slice thickness 1.25 mm, field of view 300 mm, pixel size 0.59×0.59 mm. Subsequently, a single-bed brain PET dataset, not relevant for the present study, was acquired for 20 minutes.

Immediately after the PET/CT scan, patients were transferred to the integrated PET/MR scanner (SIGNA PET/MR, GE Healthcare). There was no additional radiotracer injection for the PET/MR. The acquisition took place 76 ± 20 min, range 57 to 113 minutes, after tracer administration. The patient setup included a 32-channel brain coil (Nova Medical Inc., Wilmington, MA). A 40-minute PET acquisition was performed.

A number of MR sequences were acquired simultaneously with the PET acquisition. For attenuation correction purposes, the default LAVA-Flex sequence [21] was automatically prescribed by the system: axial acquisition, repetition time ~ 4 ms, echo time 1.12 ms & 2.23 ms, flip angle 5° , slice thickness 5.2 mm, matrix $256 \times 256 \times 120$, voxel size $1.95 \times 1.95 \times 2.60$ mm, number of averages 0.7, acquisition time: 18 s. Additionally, a prototype zero echo time (ZTE) sequence was acquired for bone identification (25): 3D radial acquisition, flip angle 0.8° , matrix $110 \times 110 \times 116$, voxel size $2.4 \times 2.4 \times 2.4$ mm, number of averages 4, bandwidth ± 62.5 kHz, acquisition time 42 s. Several diagnostic sequences were included in the protocol (e.g. T1 BRAVO, T2 CUBE, FOCUS DWI, etc.). All acquisitions used body coil transmit and the 32-channel brain coil for receive, except the attenuation correction LAVA-Flex, which used body coil transmit and receive.

C. Attenuation Map generation

For each patient, three attenuation correction (AC) maps were generated: The default atlas-based map recommended by the manufacturer for brain imaging; a ZTE-based map; and a CT-based map, to be used as gold standard.

The Atlas-AC map was generated automatically by the system's default brain PET reconstruction [22]: A non-rigid B-spline method is used to register a CT-based head atlas to the LAVA-Flex images. The resulting volume is automatically rescaled to annihilation photon attenuation coefficients and combined with templates of the bed and Nova 32-channel head coil attenuation.

The ZTE-based attenuation map was generated using a custom algorithm implemented in C++ using ITK (Kitware Inc., Clifton Park, NY): The algorithm includes pre-filtering, histogram-based normalization, intensity-based extraction of a head mask, bias correction, extraction of region of interest masks (paranasal sinuses, bone tissue, air cavities and partial volume) and pseudo-CT generation by piece-wise linear mapping of the bias-corrected ZTE intensity values [23]. Soft tissue is assigned a constant value of 42 HU, whereas bone tissue is linearly scaled based on the ZTE intensity: $pCT = 42 - 2400 \times (ZTE - 1)$. The resulting pseudo-CT is then re-sampled to the appropriate resolution for PET attenuation correction (matrix $128 \times 128 \times 89$ voxels, $4.69 \times 4.69 \times 2.78$ mm). Finally, the hardware attenuation templates are extracted from the attenuation map obtained with the Atlas method and merged into the ZTE-based map.

The CT-based attenuation map was generated using custom Matlab (Mathworks, Natick, MA) scripts: The procedure involves an interactive CT cleanup step, where unwanted structures (such as the arms and CT hardware) are removed. The resulting dataset is then automatically registered to the pseudo-CT series generated by the ZTE processing, using a rigid transform and mono-modal metric. Registration results are visually verified in each case (this simple method has been found to be robust and accurate for the cranium). The remaining steps are equivalent to those used to transform the ZTE pseudo-CTs into attenuation maps.

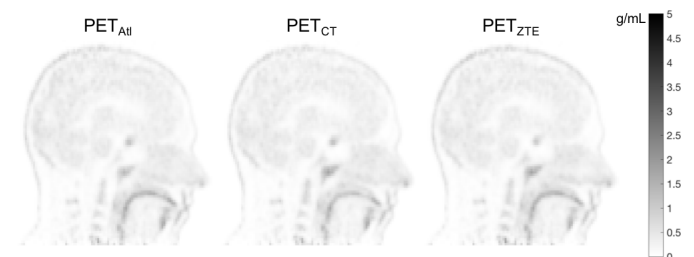


Fig. 1. Sagittal views of the reconstructed ^{11}C -Methionine PET images using each of the attenuation correction methods. Notice the hot spot on the pituitary gland.

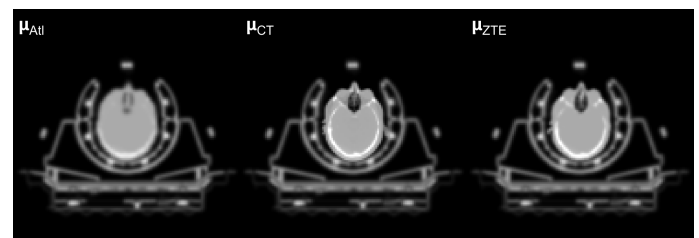


Fig. 2. Axial views of the final attenuation maps generated with each of the tested methods.

D. Retrospective PET reconstruction

PET/MR sinogram data were retrospectively reconstructed using a Matlab toolbox provided by GE Healthcare, which implements the same reconstruction algorithms used in the scanner. A separate reconstruction was performed with each of the three attenuation maps (PET_{at} , PET_{zte} and PET_{ct}). The reconstruction parameters were selected to mimic those of the PET/CT clinical protocol, while accounting for the limitations imposed by the different detector geometry: Fully 3D ordered subsets expectation maximization algorithm with time-of-flight information (VFPX), iterations 9, subsets 8, matrix $128 \times 128 \times 89$, voxel size $2.34 \times 2.34 \times 2.78$ mm³, transaxial post-reconstruction Gaussian filter 4mm, axial filter 1:2:1, point-spread function, normalization, randoms, scatter, dead-time and decay corrections.

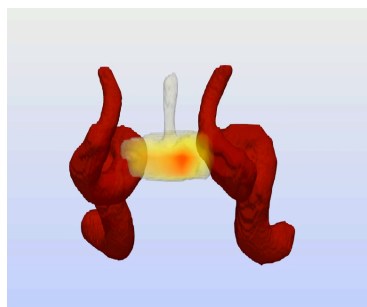


Fig. 3. Surface rendering of a pituitary gland, segmented from MR, fused with the corresponding ¹¹C-Met PET uptake. Notice how PET clearly indicates the laterality of the lesion, with respect to the centrally-located pituitary stalk. Surface renderings of the carotid arteries are provided for surgical guidance.

RESULTS

All exams were successfully completed without relevant incidents. The automated post-processing and reconstruction steps performed as expected without the need for manual corrections. Fig. 1 illustrates the results of a ¹¹C-Met PET reconstruction, with each attenuation map.

The initial ZTE processing was found to over-estimate the axial sensitivity range of the brain coil by ~1 cm and had to be fixed. Aside from this, no gross abnormalities or artifacts were detected on the attenuation maps. Figure 2 shows an example of the attenuation maps obtained with each of the three methods.

The reconstructed PET images were reviewed by an endocrinologist (W.B) and a radionuclide radiologist (I.M.), both with prior experience reading pituitary PET data, to determine the presence and location of Methionine-avid lesions. All reconstructions were judged to be suitable for the purpose of diagnosis of the pituitary. Figure 3 shows an example of pathological ¹¹C-Met PET uptake overlaid on MR-based surface renderings of the pituitary gland and carotid arteries. The identified pathologies included Cushing's disease (48%), thyrotropin-secreting pituitary adenoma (20%), acromegaly (12%), non-functioning pituitary adenoma (12%), prolactinoma (4%). Tumor volumes ranged from 195 mm³ to 6702 mm³, with an average of 1452 mm³ and median of 375 mm³.

Voxel-wise difference images between the PET images reconstructed with MR-based attenuation correction methods (PET_{at} , PET_{zte}) and the reference reconstruction using CT-based attenuation correction (PET_{ct}) were calculated. Figure 4 shows the obtained differences for a representative case. While a consistent improvement in brain uptake accuracy was appreciated for the ZTE-based method, consistent with previous reported studies [23], [24], the results were more erratic in the pituitary region, with moderate improvements and some instances of increased error near anatomical boundaries.

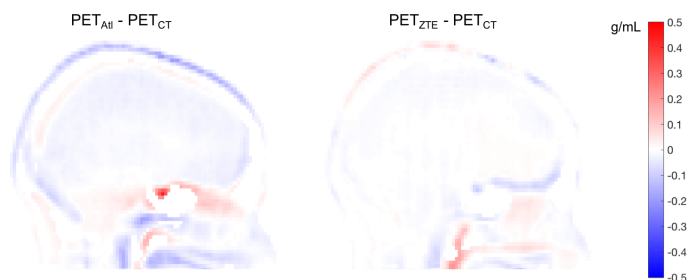


Fig. 4. Sagittal views of the differences in uptake between PET images reconstructed with each of the MR-based attenuation correction methods and the reference PET reconstruction with CT-based attenuation correction.

To obtain bias measurements specific to the region of interest, the pituitary gland and cerebellum were manually segmented on MR FSPGR images. The resulting masks were used to generate normalized uptake (SUVR) measurements. For each PET reconstruction, the mean and maximum uptake on the pituitary gland were calculated, as well as the average position of the hot-spot relative to the pituitary gland mask. Figure 5 summarizes the obtained mean SUVR results. Those cases without a clear hot-spot (7 of 25) were discarded from the subsequent analysis.

Relative differences in uptake were calculated as:

$$D_x\% = 100 \frac{SUVR_x - SUVR_{CT}}{SUVR_{CT}}$$

The reconstructions with the ZTE-based method were found to match the reference (PET_{ct}) in terms of mean SUVR with similar accuracy as their atlas-based counterparts, but considerably more precision. Tables I and II summarize these findings.

Shifts larger than 10% between the average lesion positions were identified in five cases: twice in PET_{at} , twice PET_{zte} and once in both (with the same value). Visual inspection of these cases showed low-frequency modulations of the reconstructed uptake, not likely to alter a radiologist's perception of the hot-spot.

TABLE I
MEAN UPTAKE RELATIVE DIFFERENCES W.R.T. CT REFERENCE

	SUV _{MEAN}		SUVR _{MEAN}	
	Atlas	ZTE	Atlas	ZTE
Mean	-1%	-6%	+6%	-5%
Stdv.	+17%	+8%	+16%	+8%
Min	-29%	-23%	-22%	-22%
Max	+37%	+7%	+40%	+12%
Trend	y=0.99x	y=0.95x	y=1.06x	y=0.96x
R ²	0.93	0.98	0.80	0.92

TABLE II
MAX UPTAKE RELATIVE DIFFERENCES W.R.T. CT REFERENCE

	SUV _{MAX}		SUVR _{MAX}	
	Atlas	ZTE	Atlas	ZTE
Mean	-1%	-5%	+5%	-4%
Stdv.	+14%	+7%	+13%	+8%
Min	-25%	-24%	-17%	-23%
Max	+32%	5%	+35%	+16%
Trend	y=1.04x	y=0.97x	y=1.04x	y=0.98x
R ²	0.88	0.93	0.77	0.90

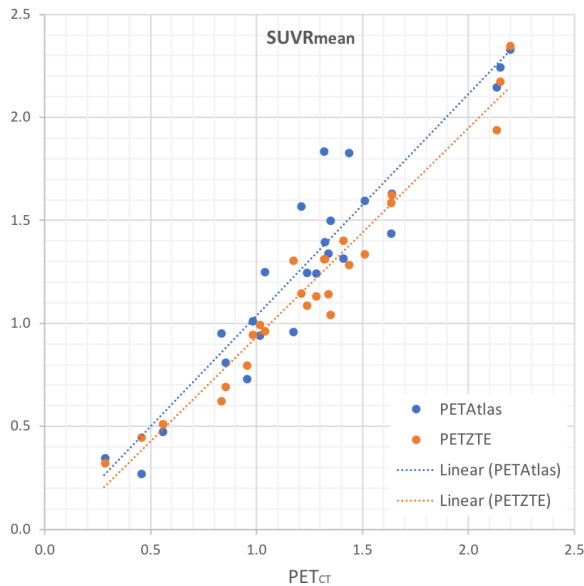


Fig. 5. Scatter plot of the pituitary mean SUVR values obtained, for each subject, with the MR-based attenuation correction methods (abscissae), compared to the CT-based reference method (ordinate).

DISCUSSION

This is the first reported clinical evaluation of the impact of advanced attenuation correction methods on PET/MR pituitary tumor diagnosis. The results suggest that attenuation correction using zero echo time MR sequences does indeed improve the accuracy of ¹¹C-Methionine PET imaging with respect to the current default atlas method.

Accurate lesion localization within the pituitary gland was possible with the proposed protocol. The availability of simultaneously acquired, well-aligned high-resolution morphological information from MR facilitated the interpretation and quantitative analysis of PET findings. This is of particular relevance, given the critical nature of transsphenoidal surgical excision: both incomplete tumor removal and excessive removal of healthy pituitary tissue result in permanent sequelae requiring costly medication and severely affecting quality of life. Accurate identification of the adenoma with PET within the high-resolution anatomical context provided by MR can be instrumental for successful surgical guidance.

While the results confirm that ZTE-based attenuation correction offers increased accuracy compared to the default atlas-based method, the improvement is neither as marked nor as consistent as in previously reported studies [25]–[27]. This is due to the challenging location of the pituitary gland, directly behind the nasal passages and above the sphenoid sinus. These are known to be difficult regions for the pseudo-CT generation algorithm, due to the abundance of air-tissue interfaces where partial volume effects are susceptible of being misclassified as bone. A potential solution to this problem is the use of novel Deep Learning algorithms, which have been recently shown to provide very promising segmentation results for this area [28].

Further work will be aimed at improving the resolution of the bone maps, in order to achieve not only more accurate attenuation correction -by drastically reducing the partial volume effect- but also potentially useful bone maps for surgical planning.

REFERENCES

[1] Q. T. Ostrom *et al.*, “CBTRUS Statistical Report: Primary brain and other central nervous system tumors diagnosed in the United States in 2010–2014,” *Neuro-Oncol.*, vol. 19, no. suppl_5, pp. v1–v88, 2017.

[2] O. Koulouri *et al.*, “Successful treatment of residual pituitary adenoma in persistent acromegaly following localisation by ¹¹C-methionine PET co-registered with MRI,” *Eur J Endocrinol*, vol. 175, no. 5, pp. 485–498, Nov. 2016.

[3] O. Koulouri *et al.*, “A role for ¹¹C-methionine PET imaging in ACTH-dependent Cushing’s syndrome,” *Eur J Endocrinol*, vol. 173, no. 4, pp. M107–20, Oct. 2015.

[4] N. Taku, O. Koulouri, D. Scoffings, M. Gurnell, and N. Burnet, “The use of (¹¹C)methionine positron emission tomography (PET) imaging to enhance radiotherapy planning in the treatment of a giant, invasive pituitary adenoma,” *BJR Case Rep.*, vol. 3, no. 2, p. 20160098, 2017.

[5] A. Martinez-Moller *et al.*, “Tissue classification as a potential approach for attenuation correction in whole-body PET/MRI: evaluation with PET/CT data,” *J Nucl Med*, vol. 50, no. 4, pp. 520–6, Apr. 2009.

[6] M. Hofmann, B. Pichler, B. Scholkopf, and T. Beyer, “Towards quantitative PET/MRI: a review of MR-based attenuation correction techniques,” *Eur J Nucl Med Mol Imaging*, vol. 36 Suppl 1, pp. S93–104, Mar. 2009.

[7] F. L. Andersen *et al.*, “Combined PET/MR imaging in neurology: MR-based attenuation correction implies a strong spatial bias when ignoring bone,” *Neuroimage*, vol. 84, pp. 206–16, Jan. 2014.

[8] J. Du and G. M. Bydder, “Qualitative and quantitative ultrashort-TE MRI of cortical bone,” *NMR Biomed*, vol. 26, no. 5, pp. 489–506, May 2013.

[9] M. Hofmann *et al.*, “MRI-based attenuation correction for PET/MRI: a novel approach combining pattern recognition and atlas registration,” *J Nucl Med*, vol. 49, no. 11, pp. 1875–83, Nov. 2008.

[10] H. Qian *et al.*, “Whole-body PET/MR attenuation correction on a sequential, tri-modality PET/CT and MR imaging setup combining image segmentation, truncation completion and atlas-based skull segmentation,” *Proc. New Paradig. Mol. Imaging Conf. Elba Italy Tuesday 29th May*, 2012.

[11] I. B. Malone, R. E. Ansorge, G. B. Williams, P. J. Nestor, T. A. Carpenter, and T. D. Fryer, “Attenuation correction methods suitable for brain imaging with a PET/MRI scanner: a comparison of tissue atlas and template attenuation map approaches,” *J Nucl Med*, vol. 52, no. 7, pp. 1142–9, Jul. 2011.

[12] I. Bezrukov *et al.*, “Quantitative Evaluation of Segmentation- and Atlas-Based Attenuation Correction for PET/MR on Pediatric Patients,” *J Nucl Med*, vol. 56, no. 7, pp. 1067–74, Jul. 2015.

[13] D. H. Paulus *et al.*, “Whole-Body PET/MR Imaging: Quantitative Evaluation of a Novel Model-Based MR Attenuation Correction Method Including Bone,” *J Nucl Med*, vol. 56, no. 7, pp. 1061–6, Jul. 2015.

[14] T. Koesters *et al.*, “Dixon Sequence with Superimposed Model-Based Bone Compartment Provides Highly Accurate PET/MR Attenuation Correction of the Brain,” *J Nucl Med*, vol. 57, no. 6, pp. 918–24, Jun. 2016.

[15] T. Sekine *et al.*, “Evaluation of Atlas-Based Attenuation Correction for Integrated PET/MR in Human Brain: Application of a Head Atlas and Comparison to True CT-Based Attenuation Correction,” *J Nucl Med*, vol. 57, no. 2, pp. 215–20, Feb. 2016.

[16] M. D. Robson and G. M. Bydder, “Clinical ultrashort echo time imaging of bone and other connective tissues,” *NMR Biomed*, vol. 19, no. 7, pp. 765–80, Nov. 2006.

[17] C. Catana *et al.*, “Toward implementing an MRI-based PET attenuation-correction method for neurologic studies on the MR-PET brain prototype,” *J Nucl Med*, vol. 51, no. 9, pp. 1431–8, Sep. 2010.

[18] D. P. Madio and I. J. Lowe, “Ultra-fast imaging using low flip angles and FIDs,” *Magn Reson Med*, vol. 34, no. 4, pp. 525–9, Oct. 1995.

[19] F. Wiesinger *et al.*, “Zero TE MR bone imaging in the head,” *Magn Reson Med*, vol. 75, no. 1, pp. 107–14, Jan. 2016.

[20] G. Delso *et al.*, “Clinical evaluation of zero-echo-time MR imaging for the segmentation of the skull,” *J Nucl Med*, vol. 56, no. 3, pp. 417–22, Mar. 2015.

[21] S. D. Wollenweber *et al.*, “Comparison of 4-class and continuous fat/water methods for whole-body, MR-based PET attenuation correction,” presented at the IEEE Nuclear Science Symposium and Medical Imaging Conference, 2012, pp. 3019–3025.

[22] S. D. Wollenweber *et al.*, “Evaluation of an Atlas-Based PET Head Attenuation Correction Using PET/CT & MR Patient Data,” *IEEE Trans. Nucl. Sci.*, vol. 60, no. 5, pp. 3383–3390, 2013.

[23] F. Wiesinger *et al.*, “Zero TE-based pseudo-CT image conversion in the head and its application in PET/MR attenuation correction and MR-

- guided radiation therapy planning,” *Magn Reson Med*, vol. 00, pp. 1–12, Feb. 2018.
- [24] G. Delso, B. Kemp, S. Kaushik, F. Wiesinger, and T. Sekine, “Improving PET/MR brain quantitation with template-enhanced ZTE,” *NeuroImage*, vol. 181, pp. 403–413, Nov. 2018.
- [25] M. Khalifé, M. Soussan, S. Desarnaud, L. Kallou, V. Brulon, and C. Comtat, “Correcting photon attenuation in brain PET-MR using a ZTE sequence and comparison to CT-based attenuation correction,” *J. Nucl. Med.*, vol. 57, no. supplement 2, p. 1871, May 2016.
- [26] G. Schramm *et al.*, “Validation of ZTE head attenuation correction in the GE SIGNA PET/MR - initial results,” *J. Nucl. Med.*, vol. 58, no. supplement 1, p. 644, May 2017.
- [27] J. Yang *et al.*, “Evaluation of Sinus/Edge-Corrected Zero-Echo-Time-Based Attenuation Correction in Brain PET/MRI,” *J Nucl Med*, vol. 58, no. 11, pp. 1873–1879, Nov. 2017.
- [28] S. Kaushik *et al.*, “Deep Learning based pseudo-CT estimation using ZTE and Dixon MR images for PET attenuation correction,” presented at the International Society for Magnetic Resonance in Medicine, Annual Meeting, Honolulu (HI), 2017.